2020 BX_{12}: THE LAST BINARY ASTEROID DISCOVERED BY ARECIBO OBSERVATORY Luisa Fernanda Zambrano Marin[1,2], P.A. Taylor[3], S.E. Marshall[1], A. McGilvray[1], F.C.F. Venditti[1], M. Devogèle[2]; [1]Arecibo Observatory, University of Central Florida, HC 3 BOX 53995, 00612, Arecibo, Puerto Rico; [2]Universidad de Granada, Escuela Internacional de Posgrado, Facultad de Ciencias, Tecnologías e Ingenierías, c/ Paz 18, 18071 Granada, Spain;luisafz@aosa.naic.edu; [3]National Radio Astronomy Observatory, Green Bank Observatory, 1180 Boxwood Estate Rd., Charlottesville, VA 22903 USA.

Keywords: *Planetary Radar, PHA, NEO*

Introduction:

Over the course of its 40-year operation, the Arecibo Observatory (AO) Planetary Radar discovered or confirmed the existence of almost 60 binary or triple near-Earth asteroid (NEA) systems. This is an impressive number, considering that the first binary asteroid was only discovered in 1993, 243 Ida with its companion Dactyl. Since then, hundreds of binary asteroids have been discovered using various methods, including ground-based observations, spacecraft flybys, and radar imaging. It is estimated that around 15% of near-Earth asteroids have companions [1].

One of the most effective techniques for the ground-based study of NEAs is radar observations. This remote sensing technique allows for precise measurements of the object's position, velocity, and size, as well as providing information on their shape, rotation, and composition [2, 3, 4]. Radar observations can unequivocally detect companion objects, which are of great interest because they can provide information on the objects' masses, densities, and internal structures. The Arecibo Observatory, located in Puerto Rico, was a key facility for planetary radar observations until the collapse of its 900 ton instrument platform on December 1, 2020. The facility was instrumental in the discovery and characterization of binary asteroids, as well as studies of other near-Earth objects (NEOs), main-belt Asteroids (MBAs), and planets and, in some cases, for spacecraft support.

The purpose of this paper is to present the initial results of these radar observations and to provide insights into the physical properties of the asteroid.

Discovery:

Asteroid 2020 BX12 was discovered on January 27, 2020, by the Asteroid Terrestrial-impact Last Alert System (ATLAS) survey at Mauna Loa Observatory [5]. The absolute magnitude (H) reported at discovery was of 20.6; an optical geometric albedo of 0.2 is usually initially used, giving an estimated diameter (D) of 222 m. The object is described as a potentially hazardous asteroid (PHA) due to its size and Earth minimum orbit intersection distance of 0.0021 au as well as its close approach of 0.0292 au on February 3, 2020. Its next close approach will occur on January 31, 2101, at 0.045 au.

Radar Observations:

The radar observations, carried out with the S-band planetary radar system (2380 MHz, 12.6 cm) at the Arecibo Observatory on February 4 and 5, 2020, immediately revealed that 2020 BX_{12} was a binary asteroid system (Fig 1). The measurement of the Doppler frequency shift and the Doppler spectrum bandwidth obtained from continuous-wave observations with the system provided incredibly sensitive astrometric corrections and initial limits for the object's apparent diameter and period of rotation.

At peak performance, the AO S-band radar was capable of transmitting up to 1 MW of power and had a receiving antenna 305 m in diameter, making it not only the world's most powerful transmitter system but also the most sensitive. Radar observations at AO utilized monochromatic circularly polarized waveforms, which could be phase modulated or unmodulated, and their echoes were received in both the same-sense (SC) and opposite-sense (OC) circular polarization as transmitted. The received echoes provide information on the object's diameter, rotation period, near-surface properties, and astrometry [6]. Radar observations usually began by a continuous-wave measurement to obtain the Doppler frequency spectrum of the echo. The Doppler shift of the location of the center of mass of the asteroid relative to the Doppler frequency of the signal, due to the motion of the target, provides a measurement of the object's line-of-sight velocity.

In the case of an offset in the expected location of the object from that predicted by the ephemeris in use, astrometric corrections were promptly submitted to the JPL Horizons System. In some cases, line-of-sight velocity corrections are on the order of meters per second [2] and used to produce a new orbital solution.

From the bandwidth measurement, we can place limits for the rotation period and the object's apparent diameter. From the unmodulated continuous-

Table 1 Radar Observations of Asteroid 2020 BX$_{12}$

UT Date	Eph	RTT	P$_{tx}$	Baud	Spb	Code	Start-Stop	Runs
2020-02-04	6	33	297	cw		none	201217-202130	9
	7		288	4	2	8191	202657-203430	6
			292	4	2	1023	203648-204137	5
	8		299	0.05	1	65535	205224-220738	67
2020-02-05	8	41	315	cw		none	192745-193107	3
		42	348	0.2	4	65535	194100-204102	36

Note: The first column indicates the universal-time date on which the observation began. Eph is the ephemeris solution number used. RTT is the round-trip light time to the target. P$_{tx}$ is the transmitter power. Baud is the delay resolution of the pseudo-random code used for imaging; baud does not apply to cw data. Spb is the number of complex samples per baud giving an effective delay resolution of baud/spb; cw data are typically sampled at a rate of 12.5 kHz. Code is the length (in bauds) of the pseudo-random code used. The timespan of the received data is listed by the UT start and stop times. Runs is the number of completed transmit-receive cycles.

wave (CW) observations, the Doppler echo-power spectra measured is used to determine the radar cross section in each polarization, σ_{OC} and σ_{SC}, which are related to the physical properties of the target [4, 7, 8]. The ratio of these cross section values is known as the the circular polarization ratio ($\mu_C = \sigma_{SC}/\sigma_{OC}$).

For targets with a relatively high signal-to-noise-ratio (SNR), we use phase modulation of the transmitted signal to produce delay-Doppler images with range resolution as fine as 7.5 m per pixel in some cases. These images aid in the estimation of object's diameter, rotation rate and in some cases, provide an insight of the body's shape [7, 9]. Table 1 provides details of the observations, including specific times, ephemeris used, distance to object as round-trip light travel time, transmitter power, mode of observation, and number of transmit-receive cycles (runs) per observation mode.

Results:

Continuous-Wave Spectra:

Observations in continuous-wave (CW) spectra quickly revealed a secondary body, as a narrow echo superimposed on the broader echo of the primary component (Fig 1.a) during the first day of observation. The primary's bandwidth was about 1.6 Hz and the secondary of 0.08 Hz (barely resolved at 0.04 Hz resolution); we see an offset from the expected zero frequency of about -10.8 Hz, for which an astrometric correction was submitted. This corresponds to a correction on the line-of-sight velocity of less than one meter per second - incredibly sensitive for an object traveling at a velocity of 25 km s^{-1}!. On the second day of continuous wave observations (Fig1.b), the primary bandwidth was about 1 Hz and the secondary was essentially unresolved. The object was quickly identified at the expected Doppler frequency, obtaining only 3 scans before moving on to another observation mode.

Since the second day of observations had a noisier signal compared to the first day, we chose to use the μ_C from the first day to ensure the accuracy and validity of our results. However, it is significant to note that relying solely on data from one day may affect the reliability of the analysis, as valuable information may be present in the noisier signal from the other observation day.

The relationship between μ_C and taxonomic class has been investigated in previous studies, including the work of [10]. Based on the measured μ_C value of 0.23 from the first day of observations, the 2020 BX$_{12}$ system is most likely a C-type or an S-type object (C-type $\mu_C \approx 0.285 \pm 0.12$, S-type $\mu_C \approx 0.26 \pm 0.05$). From the measured bandwidths, and expected diameter, based on the H magnitude of the object, we calculate the rotation period of the primary to be P$_{rot} = 3\pm$ 0.4 hr and P$_{rot}$=27 $\pm$ 3 hr for the secondary.

Delay(Range)-Doppler: Following the location of the object in Doppler, we proceeded to locate it

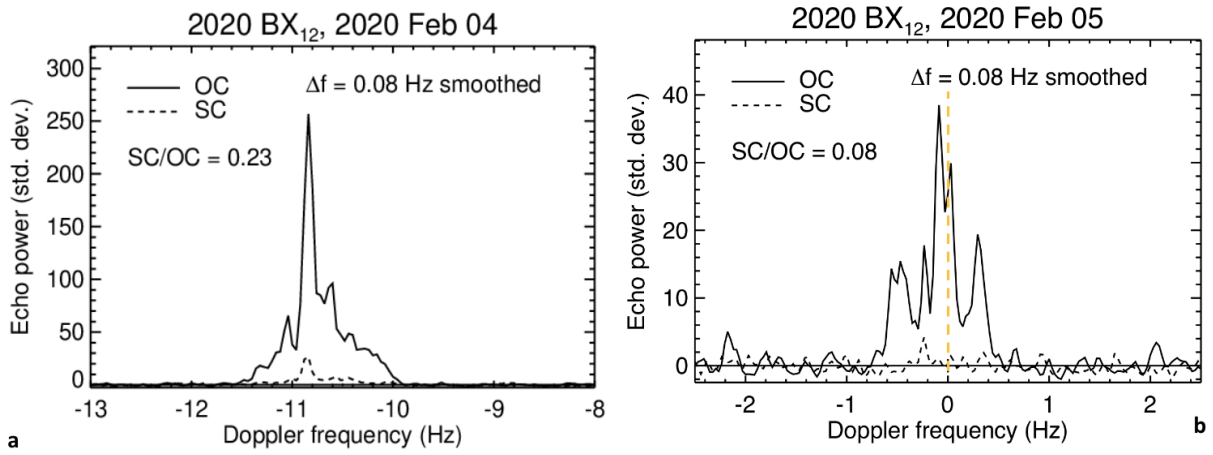

Figure 1 Continuous wave echo power spectra of both days of observation. (a) Sum of all scans for Feb 04. Secondary is clearly visible as a superposed signal of the primary. (b) Sum of all scans for Feb 05 observations, where the secondary is visible, but the data set is noisier. We discarded this day's circular polarization ratio.

in range, using a 4 μs phase modulation. We found the echo was spread over several range bins, but the components were not resolved. Following range measurements an astrometric correction of 146 μs microseconds was submitted, which corresponds to just a few kilometers on an object 27 million kilometers (0.18 au) away!

Follow-up radar imaging at 0.05 us (7.5 m px^{-1}, 0.075 Hz px^{-1} resolution, Fig. 2-left) reveal an echo appearing spheroidal in shape and roughly 160 $\pm$ 30 m diameter, based on its visible extent.

The secondary is unambiguously detected as a separate echo in the images, although the shape is unresolved, we can estimate a diameter of 70 $\pm$10 m, based on its visible extent. Nonetheless, visual estimation can sometimes underestimate or overestimate sizes, and hence, this size determination is still subject to some uncertainty. Conversely, the secondary's echo is estimated have a diameter of at least 60 m based on the visible extent. The secondary's shape is unresolved. The maximum separation observed for the two bodies was on the order of 360 $\pm$ 20 m. Notably (Fig 2), the secondary echo had near-zero Doppler, but was clearly offset to the side of the primary echo, once again indicating the presence of a slight Doppler offset in the ephemeris.

During the second day of observation, we used a coarser phase modulation for imaging. When analyzing the data at 0.2 μs (Fig. 2-right), we observe that the primary echo- considering only pixel values clearly above 3 sigma-, the visible extent of the primary echo is estimated to be 105 m, or roughly 210 m in diameter. In contrast, the secondary visible-extent echo is estimated to be a bit over 35 m, an estimated diameter of 70 m. However, it is important to note that the signal is spread over 0.2 μs with 4 samples per baud, which introduces smearing in the range dimension. This smearing may cause an overestimation of the true size of the object.

Object Dynamics:

The orbit is reported [5] to be elliptical, with an eccentricity $e = 0.53$, a semi-major axis of 1.60 au and an orbital inclination of $i = 40°$ with respect to the ecliptic plane, which means it does not deviate significantly from the plane of the Earth's orbit. Precovery images from Pan-STARRS 1, spanning six years, combined with radar data reduced its uncertainty from 8 to 1. The observation arc currently spans 8.08 years with an orbit uncertainty parameter of 0 [5]. The asteroid's orbit is stable and not expected to change significantly in the near future.

Regarding the spin rate, the asteroid's rotation around its own axis (due to sky motion), was determined to be between 13 and 19 deg day^{-1}.

The radar images in Fig 2 are roughly 24 hr apart, and show a mutual-orbital phase change by about 180 degrees, where the secondary is initially leading the primary to the secondary trailing the primary. This could support a tidally locked secondary and a mutual-orbit period of 45-50 hours, though a shorter orbital period of 15-16 hours has not been ruled out.

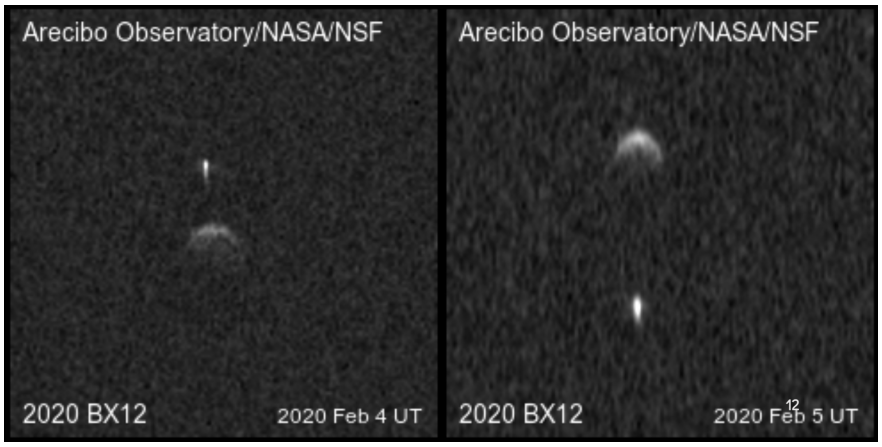

Figure 2 Delay-Doppler images of NEA/PHA 2020 BX_{12} for both days of observation. Figure on the left displays the to data acquired at phase modulation of 0.05 μs, which corresponds to a resolution of 7.5 m px^{-1} in delay and and 0.075 Hz px^{-1} in Doppler at 1 sample per baud. Image on the right has a phase modulation of 0.2 μs), corresponding to a resolution of 7.5 m px^{-1} in delay and and 0.075 Hz px^{-1} in Doppler; at 4 samples per baud.

Cohesion:

To further investigate the internal structure of 2020 BX_{12}, we follow [11, 12, 13, 14] in calculating the Drucker-Prager yield criterion, a pressure dependent measurement of the shear stress for a rotating ellipsoidal solid body right before physical deformation.

This criterion, the cohesion (k), is defined by two constants the tensile & sheer stress at zero pressure and the angle of friction ψ, which defines the change in shear strength at a confined pressure.

Using the radar-derived diameter and rotation period, assuming a spheroidal shape with an estimated volume based on the radar diameter and an angle of friction 45 degrees, we calculated k for density steps from 1 to 3 g cm^3. We obtain cohesion of less than 1 kPa, supporting our suspicion of an S-type or C-type taxonomical class.

Shape Model:

The radar observations were also used to produce preliminary shape models of 2020 BX12 (Fig 3). Using the SHAPE software [15, 16, 17], we compared the radar data to simulated observations for models with a variety of possible sizes and rotation states.

We are initially modeling the primary as an ellipsoid, and without any lightcurve data our models are not well constrained. The pole direction could be almost anywhere on the celestial sphere, we present two of such models in Figure 3.

Conclusions:

The Arecibo Observatory's schedule adaptability allowed for a quick request of telescope time for this observation. As soon as the object was within its field of view, observations were carried out on February 04 and February 05, 2020. Within minutes, the object was found to be a binary system. The rotation period of a few hours, a diameter of a few hundred meters and an average cohesion of a few hundred pascals, can indicate 2020 BX_{12} is an average body within the the general population of binary asteroids.

The primary component seems to have an spheroidal shape, and although the secondary's shape is unresolved, its roughly half of the visible extent derived diameter of the primary. Table 2 presets a summary of the radar derived physical and dynamical characteristics of this object.

Further analysis of this data set and acquisition of new observations of this system will be needed to fully understand its properties and evolution. However, the February 2020 apparition was the closest this object will be in the next 100 years [5]. Its next apparition in February 2024 will present an opportunity for performing observing campaigns. There are currently no light-curve data available for this object. Having those types of measurements will greatly improve shape modeling efforts. These observations could include additional radar imaging during its next close approach on February 20204 to refine estimates of the asteroid's size and shape, these could as well be spectroscopic observations and photometry to determine its composition. Additionally, monitoring

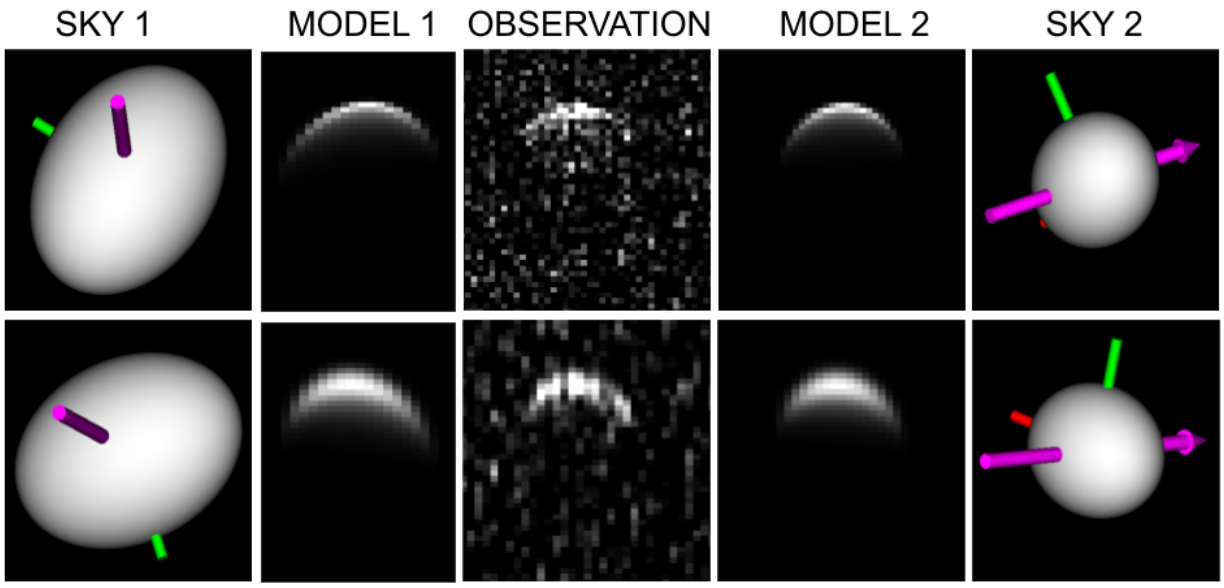

Figure 3 The image displays two ellipsoid models chosen from many possibilities. The first model, located on the left (sky 1), has dimensions of 350 x 260 x 250 m and a rotation period of 2.2 hours, with a pole at ecliptic coordinates (10, +10). The second model, on the right, has dimensions of 220 x 190 x 180 m and a rotation period of 2.8 hours, with a pole at ecliptic coordinates (334, +40). Both data and synthetic-echo images show a downward increase in delay and a rightward increase in frequency (Doppler). The plane-of-sky images are oriented with celestial north towards the top and east towards the left. The colored rods mark the principal axes of inertia, where red represents the minimum inertia axis and green represents the intermediate axis. The purple arrow points to the rotation vector, which aligns with the axis of maximum inertia.

the asteroid's orbit over time could reveal any unexpected changes in its trajectory due to gravitational interactions with other objects in the Solar System. The loss of the Arecibo Observatory severely hinders our ability to rapidly discover and characterize secondary or additional bodies accompanying NEAs. Ground-based instruments such as the Arecibo Observatory could provide so much information about NEA/PHA's physical and dynamical properties, allowing us to prepare the appropriate deflection mechanism when needed. The loss of a tool of this magnitude and sensitivity is truly a setback in our efforts to understand these objects.

Acknowledgements:
The Arecibo Planetary Radar Program is fully supported by NASA's Near-Earth Object Observations Program in NASA's Planetary Defense Coordination Office through grant no. 80NSSC19K0523 awarded to University of Central Florida (UCF). UCF manages the National Science Foundation facility under a cooperative agreement with Yang Enterprises, Inc. and Universidad Ana G. Méndez.

Table 2 Radar derived values for some physical and dynamical properties for the 2020 BX_{12} system.

Parameter	Value
Primary Maximum Diameter	270 $\pm$ 90 m
Secondary Maximum Diameter	70 $\pm$ 30 m
Primary P_{rot}	2.5 $\pm$ 1 hr
Secondary P_{rot}	25 $\pm$ 5 hr
Class	S or C-type
Primary μ_C (CPR)	0.23
Projected Separation	360 $\pm$ 15 m
Primary Cohesion	500 $\pm$ 200 Pa

References: [1] P. Pravec, et al. (2007) *Icarus* 190(1):250 ISSN 0019-1035 doi. [2] Ostro, Steven J (1997) *Engineering and Science* 60(2):14. [3] G. J. Black (2002) in *Single-Dish Radio Astronomy: Techniques and Applications* vol. 278 271–290. [link]. [4] A. Virkki, et al. (2016) *Icarus* 269:38 doi. [5] Horizons web-interface https://ssd.jpl.nasa.gov/horizons/ accessed: March 17, 2023. [6] S. J. Ostro (1993) *Reviews of Modern Physics* 65(4):1235 doi. [7] A. K. Virkki, et al. (2022) *The Planetary Science Journal* 3(9):222 doi. [8] C. Magri, et al. (2007) *Icarus* 186(1):126 doi. [9] M. C. Nolan, et al. (2013) *Icarus* 226(1):629 doi. [10] L. A. Benner, et al. (2008) *Icarus* 198(2):294 doi. [11] D. Polishook, et al. (2016) *Icarus* 267:243 doi. [12] D. Polishook, et al. (2017) *Icarus* 297:126 doi. [13] K. A. Holsapple (2007) *Icarus* 187(2):500 doi. [14] L. F. Zambrano-Marin, et al. (2022) *The Planetary Science Journal* 3(6):138 doi. [15] C. Magri, et al. (2007) *Icarus* 186(1):152. [16] S. Hudson (1994) *Remote Sensing Reviews* 8(1-3):195. [17] A. Rożek, et al. (2019) *Astronomy & Astrophysics* 631:A149.